Magnetic excitations in nuclei with neutron excess

G. Co', V. De Donno

Dipartimento di Fisica, Università del Salento and,

INFN Sezione di Lecce, Via Arnesano, I-73100 Lecce, ITALY

M. Anguiano, A. M. Lallena

Departamento de Física Atómica, Molecular y Nuclear,

Universidad de Granada, E-18071 Granada, SPAIN

(Dated: December 14, 2011)

Abstract

The excitation of the 1^+, 2^- and 3^+ modes in ^{16}O, ^{22}O, ^{24}O, ^{28}O, ^{40}Ca, ^{48}Ca, ^{52}Ca and ^{60}Ca nuclei is studied with self-consistent random phase approximation calculations. Finite-range interactions of Gogny type, containing also tensor-isospin terms, are used. We analyze the evolution of the magnetic resonances with the increasing number of neutrons, the relevance of collective effects, the need of a correct treatment of the continuum and the role of the tensor force.

PACS numbers: 21.60.Jz, 25.20.Dc, 25.30.Dh, 25.30.Fj

I. INTRODUCTION

The possibility offered by the new radioactive ion beam facilities to produce nuclei with neutron excess opens new perspectives in the study of nuclear excitations. Recently, we have investigated the electric, natural parity, excitations of these nuclei by using a self-consistent continuum Random Phase Approximation (CRPA) approach [1, 2]. In self-consistent approaches, the single particle (s.p.) wave functions and energies are obtained by solving the Hartree-Fock (HF) equations with the same effective interaction used in the RPA calculations. The values of the parameters of these interactions are chosen to reproduce some ground state properties of a large number of nuclei. These fits produce universal parameterizations of the force to be used for all nuclei, even for those not yet explored by the experiment.

Self-consistent RPA approaches have greater prediction power than their phenomenological counterparts, but they require a higher level of accuracy in the calculations. For example, the dimension of the s.p. configuration space, beyond a certain size, is not a problem in phenomenological approaches since the effects of the truncation of the s.p. basis are taken into account by changing the values of the interaction parameters. This procedure cannot be used in self-consistent approaches, because the interaction parameters are chosen once forever. This drawback of the self-consistent RPA approach is avoided if the full s.p. configuration space is used in the calculation. This implies a proper treatment of the continuum part of the s.p. spectrum.

In this work we present the results of our study of magnetic, unnatural parity, excitations, conducted with our self-consistent CRPA approach. Since magnetic excitations are modes where nucleons with different spin orientations vibrate ones against the other ones, it is obvious that the restoring force is related to the spin-dependent terms of the nuclear interaction. Microscopically, the most important term of this part of the interaction is generated by one-pion exchange, which is the longest range part of the interaction, and has a tensor spin-isospin dependent component. This means that a realistic description of magnetic excitations requires an effective interaction which has both finite-range and tensor components. The CRPA approach we have developed allows us to consider both these characteristics without any approximation.

We carried out our calculations by using finite range forces of Gogny type. These inter-

actions have been parameterized to reproduce the binding energy of almost two thousand nuclei and the root mean square charge radii of hundreds of them. In addition, also some nuclear matter properties and fission thresholds have been included in the fit procedure [3, 4]. In our work we used the traditional D1S [5] and D1M [6] interactions and the D1ST and D1MT forces we have recently constructed by adding a tensor-isospin term to the former two parameterizations [7].

We have conducted our investigation in various oxygen and calcium isotopes where the s.p. levels below the Fermi surface are fully occupied, and those above are empty. These isotopes are spherical. Furthermore, we have verified the relevance of the pairing by doing BCS calculations. We found presence of pairing effects only in ^{22}O and ^{52}Ca nuclei, where they are, however, so small, few parts on a thousand in binding energies and root mean squared radii, that we neglected them in our study.

In this presentation we focus our attention on the following points:

1. the evolution of the strength distribution of a specific magnetic multipole excitation with increasing neutron number,

2. the relevance of collective effects,

3. the need of a correct description of the continuum, and

4. the role of the tensor force.

In Sec. II we briefly recall the main features of our CRPA approach and we give the basic expressions of the observables calculated. In Sect. III we describe the interactions and the various types of calculations we have used in our investigation. In Sec. IV we present a selected set of the results we have obtained. We first discuss the excitation of the 1^+ mode, then we consider the 2^- and 3^+ excitations. We summarize our main results and we draw our conclusions in Sec. V.

II. FORMALISM

In this section we present the basic ideas of the method we use to solve the CRPA equations. A detailed presentation can be found in Ref. [1].

The starting point of the CRPA theory is the expression of the operator that applied to the ground state generates the excited state $|\nu\rangle$:

$$Q^\dagger_\nu \,=\, \sum_{ph} \sum\!\!\!\!\!\!\int_{\epsilon_p} \Big[X^\nu_{ph}(\epsilon_p)\, a^\dagger_p(\epsilon_p)\, a_h \,-\, Y^\nu_{ph}(\epsilon_p)\, a^\dagger_h\, a_p(\epsilon_p) \Big] \,, \tag{1}$$

where we have indicated with $a^\dagger$ and a the usual particle creation and annihilation operators and with X^ν_{ph} and Y^ν_{ph} the RPA amplitudes. In the above equation we have explicitly indicated the dependence upon the variable ϵ_p, the energy of the particle state. We have indicated with the label p the orbital and total angular momentum quantum numbers. The symbol $\sum\!\!\!\!\!\!\int$ indicates a sum on the discrete values of ϵ_p and an integration on the continuous ones. The symbol h indicates all the quantum numbers characterizing a state below the Fermi surface, a hole state, including its energy, which assumes discrete values only.

The CRPA secular equations whose solution provides the values of X and Y can be written as

$$\begin{aligned}
&(\epsilon_p - \epsilon_h - \omega)\, X^\nu_{ph}(\epsilon_p) + \\
&\qquad \sum_{p'h'} \sum\!\!\!\!\!\!\int_{\epsilon_{p'}} \Big[v^J_{ph,p'h'}(\epsilon_p,\epsilon_{p'})\, X^\nu_{p'h'}(\epsilon_{p'}) \,+\, u^J_{ph,p'h'}(\epsilon_p,\epsilon_{p'})\, Y^\nu_{p'h'}(\epsilon_{p'}) \Big] \,=\, 0 \,, \qquad (2) \\
&(\epsilon_p - \epsilon_h + \omega)\, Y^\nu_{ph}(\epsilon_p) + \\
&\qquad \sum_{p'h'} \sum\!\!\!\!\!\!\int_{\epsilon_{p'}} \Big[v^{J*}_{ph,p'h'}(\epsilon_p,\epsilon_{p'})\, Y^\nu_{p'h'}(\epsilon_p) \,+\, u^{J*}_{ph,p'h'}(\epsilon_p,\epsilon_{p'})\, X^\nu_{p'h'}(\epsilon_{p'}) \Big] \,=\, 0 \,. \qquad (3)
\end{aligned}$$

In the above equations, ω labels the excitation energy and the interaction terms have been defined as

$$v^J_{ph,p'h'}(\epsilon_p,\epsilon_{p'}) \,=\, v^{J,\mathrm{dir}}_{ph,p'h'}(\epsilon_p,\epsilon_{p'}) \,-\, v^{J,\mathrm{exc}}_{ph,p'h'}(\epsilon_p,\epsilon_{p'}) \,, \tag{4}$$

and

$$u^J_{ph,p'h'}(\epsilon_p,\epsilon_{p'}) \,=\, (-1)^{j_{p'}+j_{h'}-J}\, v^J_{ph,h'p'}(\epsilon_p,\epsilon_{p'}) \,, \tag{5}$$

with

$$v^{J,\mathrm{dir}}_{ph,p'h'}(\epsilon_p,\epsilon_{p'}) \,=\, \sum_\alpha \int d^3r_1 \int d^3r_2\, \phi^*_p(\mathbf{r}_1,\epsilon_p)\, \phi^*_{h'}(\mathbf{r}_2)\, V_\alpha(\mathbf{r}_1,\mathbf{r}_2)\, \phi_h(\mathbf{r}_1)\, \phi_{p'}(\mathbf{r}_2,\epsilon_{p'}) \,, \tag{6}$$

$$v^{J,\mathrm{exc}}_{ph,p'h'}(\epsilon_p,\epsilon_{p'}) \,=\, \sum_\alpha \int d^3r_1 \int d^3r_2\, \phi^*_p(\mathbf{r}_1,\epsilon_p)\, \phi^*_{h'}(\mathbf{r}_2)\, V_\alpha(\mathbf{r}_1,\mathbf{r}_2)\, \phi_{p'}(\mathbf{r}_1,\epsilon_{p'})\, \phi_h(\mathbf{r}_2) \tag{7}$$

Here we have indicated with ϕ the s.p. wave function.

In our calculations we consider a two-body nucleon-nucleon interaction composed by terms of the form

$$V_\alpha(\mathbf{r}_i,\mathbf{r}_j) = v_\alpha(|\mathbf{r}_i-\mathbf{r}_j|)\, O^\alpha_{i,j}\,, \quad \alpha = 1,2,\ldots,6\,, \tag{8}$$

where v_α is a scalar functions of the distance between the two interacting nucleons and O^α indicates the type of operator dependence. Specifically we have considered the following six expressions:

$$O^\alpha_{i,j} : 1\,,\ \boldsymbol{\tau}(i)\cdot\boldsymbol{\tau}(j)\,,\ \boldsymbol{\sigma}(i)\cdot\boldsymbol{\sigma}(j)\,,\ \boldsymbol{\sigma}(i)\cdot\boldsymbol{\sigma}(j)\,\boldsymbol{\tau}(i)\cdot\boldsymbol{\tau}(j)\,, S(i,j)\,,\ S(i,j)\boldsymbol{\tau}(i)\cdot\boldsymbol{\tau}(j)\,. \tag{9}$$

In the above expressions we have indicated with $\boldsymbol{\sigma}$ the Pauli matrix operator acting on the spin variable, with $\boldsymbol{\tau}$ the analogous operator for the isospin, and with

$$S(i,j) \;=\; 3\,\frac{[\boldsymbol{\sigma}(i)\cdot(\mathbf{r}_i-\mathbf{r}_j)]\,[\boldsymbol{\sigma}(j)\cdot(\mathbf{r}_i-\mathbf{r}_j)]}{(\mathbf{r}_i-\mathbf{r}_j)^2} \;-\; \boldsymbol{\sigma}(i)\cdot\boldsymbol{\sigma}(j) \tag{10}$$

the usual tensor operator. In the HF calculations we have implemented this interaction with a density dependent zero-range spin-orbit term as it is commonly done in the formulation of the Gogny interaction [8]. In our calculations the Coulomb and spin-orbit terms of the interaction are considered in HF, but neglected in RPA calculations. This breaks the complete self-consistency of our calculations, however, these two terms of the interaction produce very small effects which, in addition, have the tendency of canceling with each other [9].

The first step of our method of solving the CRPA equations (2) and (3) consists in reformulating them in terms of new unknown functions, called channel functions, which do not have an explicit dependence on the continuous s.p. energy ϵ_p:

$$f^\nu_{ph}(r) \;=\; \sum\!\!\!\!\!\!\int_{\epsilon_p} X^\nu_{ph}(\epsilon_p)\, R_p(r,\epsilon_p)\,, \tag{11}$$

and

$$g^\nu_{ph}(r) \;=\; \sum\!\!\!\!\!\!\int_{\epsilon_p} Y^{\nu *}_{ph}(\epsilon_p)\, R_p(r,\epsilon_p)\,. \tag{12}$$

In the above equations, we have indicated with R the radial part of the s.p. wavefunction.

In this new reformulation of the CRPA equations, a set of algebraic equations with unknowns depending on the continuous variable ϵ_p has been changed into a set of integro-differential equations with unknowns depending on the distance from the center of coordinates. We solve this new system of equations by expanding the channel functions f and g on a basis of Sturmian functions.

The CRPA equations are solved by imposing that the particle is emitted with specific values of energy and of orbital and total angular momenta. These quantum numbers characterize, together with the quantum numbers identifying the hole state, the so-called elastic channel p_0h_0. For a given value of ω the CRPA equations are then solved for every elastic channel p_0h_0 allowed by the energy conservation. In other words, the number of elastic channels is that of the ph pairs where the particle is in the continuum.

The solution of the CRPA equations provides the channel functions $f_{ph}^{p_0h_0}(r)$ and $g_{ph}^{p_0h_0}(r)$ that allow us to calculate the transition matrix elements induced by an operator T_J. If this operator is of one-body type, it can be expressed as

$$T_{JM}(\mathbf{r}) \;=\; \sum_{i=1}^{A} F_J(r_i)\,\theta_{JM}(\Omega_i)\,\delta(\mathbf{r}_i-\mathbf{r})\,, \tag{13}$$

where we have separated the dependence on the radial and on the angular variables. By using the above expression we can express the transition matrix element as

$$\begin{aligned}\langle J\|T_J\|0\rangle_{p_0h_0} \;=\; \sum_{ph}\Bigg[&\langle j_p\|\theta_J\|j_h\rangle\int \mathrm{d}r\, r^2\,(f_{ph}^{p_0h_0}(r))^*\,F_J(r)\,R_h(r)\\ &+(-1)^{J+j_p-j_h}\,\langle j_h\|\theta_J\|j_p\rangle\int \mathrm{d}r\, r^2\,R_h^*(r)\,F_J(r)\,g_{ph}^{p_0h_0}(r)\Bigg]\,. \end{aligned}\tag{14}$$

Here, the double bar indicates the reduced angular momentum matrix elements as defined by the Wigner-Eckart theorem which we consider with the phase convention of Ref. [10].

In the present paper, for the photon excitation of unnatural parity, magnetic, states we use the following expression for the operator T_J:

$$T_{JM} \;=\; \mu_N\sum_{i=1}^{A}\left[g_s^{(i)}\mathbf{s}_i+\frac{2}{J+1}g_l^{(i)}\mathbf{l}_i\right]\cdot\left[\nabla\mathbf{r}_i^J\mathbf{Y}_{JM}(\Omega_i)\right]\delta(\mathbf{r}_i-\mathbf{r})\,, \tag{15}$$

where $\mathbf{Y}_{JM}$ indicates the vector spherical harmonics [10], $\mu_N = e\hbar/2mc$ is the nuclear magneton and g_l and g_s are the gyromagnetic factors for orbital angular momentum and spin ($g_l = 1$, $g_s = 5.586$, for protons, and $g_l = 0$, $g_s = -3.826$, for neutrons).

For a given excitation energy ω and magnetic transition $\mathcal{M}J$ we calculated the B-value as the incoherent sum over all the elastic channels p_0h_0,

$$B(\mathcal{M}J)\uparrow = \sum_{p_0h_0}|\langle\omega, J\|T_J\|0\rangle_{p_0h_0}|^2\,. \tag{16}$$

The explicit expression of the s.p. matrix elements of the operator (15) is well known in the literature, (see, for example, Eq. (B.82) of Ref. [11]).

Eqs. (13) and (14) are very general, and we used them to evaluate inelastic electron scattering cross sections. In this case, we used the expressions of the convection and magnetization currents and those of the corresponding matrix elements given in Ref. [12].

III. DETAILS OF THE CALCULATIONS

Our calculations are based on two different parameterizations of the Gogny interaction, the more traditional D1S force [5] and the new D1M force [6] obtained from a fit to about 2000 nuclear binding energies and 700 charge radii. The D1S and D1M forces describe the empirical saturation point of symmetric nuclear matter and reproduce rather well the behavior of the equations of state calculated with microscopic approaches [13, 14]. The situation for pure neutron matter is different, because the behavior of the D1S equation of state at high densities is unphysical. The D1M force produces a neutron equation of state which has a plausible behavior at high densities, even though it does not reproduce the results of modern microscopic calculations. In addition to these two forces, we also used other two parameterizations of the Gogny force containing a tensor-isospin term, the D1ST and D1MT interactions [7]. In mean-field calculations, the inclusion of the tensor force does not modify the nuclear and neutron matter equations of state. We have constructed these interactions by adding to the corresponding Gogny parameterization a tensor-isospin term obtained by multiplying the analogous term of the microscopic Argonne V18 interaction by a function which modifies its behavior at short internucleonic distances. This function contains a single parameter whose value determines the strength of the tensor force. We have chosen the value of this parameter to reproduce the experimental energy of the first 0^- excited state, and the splitting between the s.p. energies of the neutron $(1p_{3/2})^{-1}$ and $(1p_{1/2})^{-1}$ levels in the ^{16}O nucleus. In what follows we have used the superscript -1 to indicate a hole s.p. state, i.e. below the Fermi surface.

As last detail regarding our CRPA calculations, it is worth to mention that we found convergence in our results when we included at least 10 expansion coefficients of the Sturm-Bessel basis used in the calculations.

In this work, we have compared the results obtained with discrete RPA (DRPA) calculations with those found in CRPA ones. We have described in the previous section how we solve the CRPA equations. The solution of the DRPA equations is based on the expansion

of the HF s.p. wave functions on a harmonic oscillator basis and a subsequent diagonalization of the secular equations expressed in a matrix form. The expansion on the harmonic oscillator basis imposes an exponentially decaying asymptotic behavior also to the s.p. wave functions with positive energy. This implies a discretization of the continuum that requires a truncation of the s.p. space. In our calculations we have obtained convergence in the results by using 50 harmonic oscillator expansion coefficients and s.p. energies up to 150 MeV.

In the following, we shall compare our RPA results with those of the independent particle model (IPM) obtained by switching off the residual interaction in RPA calculations. The IPM calculations have been performed in both discrete and continuum cases, and we indicate the corresponding results as DIPM and CIPM, respectively.

Our formalism is constructed to treat spherical systems. For this reason, we have chosen to study four oxygen isotopes, ^{16}O, ^{22}O, ^{24}O and ^{28}O, and four calcium isotopes, ^{40}Ca, ^{48}Ca, ^{52}Ca and ^{60}Ca, where the s.p. levels below the Fermi surface are fully occupied. In these nuclei there are not deformations and the pairing effects are negligible as indicated by the results of the deformed Hartree-Fock-Bogolioubov calculations of Ref. [15]. Recently, we have studied the ground state properties of these isotopes, and also those of other heavier nuclei, with HF calculations done with finite and zero range forces, and with relativistic Hartree calculations [16]. We have found a good convergence of the results of these three types of calculations in all the properties studied.

IV. RESULTS

In this section we present a selection of the results we have obtained in our study. The presentation is organized as follows. We first discuss, with some detail, the 1^+ excitation, especially the results obtained for the oxygen isotopes. In a following subsection we present results concerning the 2^- and 3^+ magnetic excitations.

We have carried on our calculations by using the four interactions introduced in the previous section. We have observed that the results obtained with the D1S and D1M forces are similar, as well as those obtained with the D1ST and D1MT interactions. For this reason, in the following, we shall present mainly the results obtained with the D1S and D1ST forces, eventually quoting those obtained with the other two interactions when this is relevant for

the discussion.

A. Magnetic dipole response

In Fig. 1 we compare the $B(\mathcal{M}1)\uparrow$ results for the four oxygen isotopes under investigation obtained with the D1S interaction in DRPA (dashed vertical lines) and CRPA (full lines) calculations. The positions of the peaks of the DRPA results correspond to those of the continuum responses. It is remarkable the agreement between the main peaks of the discrete and continuum responses in ^{22}O and ^{24}O. Only the results for the ^{28}O nucleus show a very broad continuum response that the discrete calculations can hardly reproduce.

A feature common to all our results is already evident in Fig. 1. The $B(\mathcal{M}1)\uparrow$ strengths in the ^{16}O and ^{28}O nuclei are orders of magnitude smaller than those of the other two isotopes. In our model, the 1^+ excitation in ^{16}O and ^{28}O is generated by $2\hbar\omega$ particle-hole (p-h) configurations, since, in the ground states of these nuclei, the nucleons fully occupy all the spin-orbit partner levels below the Fermi surface. On the contrary, in ^{22}O and ^{24}O the neutron $(1d_{3/2})$ level is empty, while the $(1d_{5/2})^{-1}$ level is occupied. In this last case, since a 1^+ transition between these two states, a $0\hbar\omega$ transition, is allowed, the corresponding $B(\mathcal{M}1)\uparrow$ strengths are much larger than those of ^{16}O and ^{28}O.

The role of the residual interaction on the energy distribution of the $B(\mathcal{M}1)\uparrow$ strengths is shown in Fig. 2 where we compare the results obtained with the D1S interaction in CIPM and CRPA calculations, shown by the dashed and full lines respectively. We observe an almost exact overlap of the two results in ^{16}O and ^{28}O nuclei. The situation is more interesting for the other two oxygen isotopes where the effective interaction pushes the peak position at higher energies and, at the same time, spreads the strength.

Further information on the role of the residual interaction is given by the total $B(\mathcal{M}1)\uparrow$ strengths of the ^{22}O and ^{24}O nuclei shown in Table I where we compare the results obtained with all the four interactions introduced in Sect. III. The total strengths of the discrete calculations have been obtained by summing all the $B(\mathcal{M}1)\uparrow$ values found in the diagonalization procedure. In the continuum cases, the values given in the table have been obtained by integrating the ^{22}O and ^{24}O strength distributions shown in the panels of Figs. 1 and 2, i.e. up to a maximum energy of 20 MeV. In the table we also show the results obtained in discrete Tamm-Dancoff calculations (DTDA) performed by switching off the

RPA terms related to the Y amplitudes.

The results shown in the table indicate that, independently from the interaction, the values of the total strengths of the DIPM and DTDA calculations are identical. The residual interaction in TDA calculations redistributes the IPM strength between the various excited states, which appear at different excitation energies, without modifying its total value. The situation changes when ground state correlations are considered. DRPA results show that the values of the total strengths are reduced with respect to those of the DIPM. This effect of the ground state correlations is evident also in the results of the continuum calculations where we found even larger reduction factors.

We show in Fig. 3 the transverse responses of the ^{22}O nucleus for an inclusive electron scattering process calculated at the peak energy with different models. The responses are shown as a function of the effective momentum transfer [17]. In these calculations we used the D1S interaction. The result of the CRPA calculation has been obtained by integrating the responses on the excitation energy below the peak. The integration limits have been chosen such as the result is numerically stable.

The results shown in the figure indicate that the differences between continuum and discrete RPA results arise mainly at high momentum values. In order to understand the source of these differences we made a DRPA calculation by using only the two main neutron p-h excitations: $[(1d_{3/2})(1d_{5/2})^{-1}]$ and $[(2d_{3/2})(1d_{5/2})^{-1}]$. The result of this calculation is shown by the dashed line, which has a rather different behavior with respect to the CRPA response for all the momentum transfer values. We performed another calculation by using DRPA wave functions where all the proton contributions have been eliminated. The result of this calculation is shown by the dotted line. In this case we observe a good agreement with the CRPA result below 2 fm^{-1}, and also the peak at about 2.7 fm^{-1} is reproduced in its gross features. This indicates that in CRPA the role of the main neutron s.p. components is enhanced with respect to DRPA. The proton contributions in DRPA affect the response at high momentum transfer since they are produced by $2\hbar\omega$ excitations that have higher Fourier components than the main neutron configurations, which are $0\hbar\omega$ excitations. In DRPA calculations, these proton contributions generate a destructive interference with those of the neutrons and lower the transverse response at large momentum transfer. A similar study in ^{24}O presents analogous features.

After discussing the role of the continuum and that of the residual interaction, we now

analyze the effects of the tensor part of the residual interaction. In Table I we compare the total $B(\mathcal{M}1)\uparrow$ strengths obtained with the tensor force, the D1ST and D1MT results, with those obtained without it, the D1S and D1M results. The effect of the tensor on the IPM strengths is negligible. More interesting are the effects on the RPA results where the inclusion of the tensor force lowers the values of the total $B(\mathcal{M}1)\uparrow$ strengths in almost all the cases we have considered, the only exception being the D1S results in ^{24}O. This last effect is probably due to the truncation of the integration at 20 MeV, since we observe that around this energy the response obtained with the tensor force drops more quickly than the other one.

The effects of the tensor force on the energy distributions of the $B(\mathcal{M}1)\uparrow$ values are shown in Fig. 4, where we show CRPA results only and, following the nomenclature of Ref. [7], we indicate with nn the results of calculations done without tensor force, with tn those where the tensor force is used only in HF calculations and not in RPA, and with tt the results obtained by using the tensor force in both HF and RPA calculations.

The results of these three calculations almost overlap for the ^{16}O and ^{28}O nuclei. We have observed that already the results of Fig. 2 indicated a small sensitivity to the full residual interaction of the 1^+ excitation in these two nuclei, therefore is not surprising that the inclusion of the tensor force does not change the situation. In addition, these results confirm that in HF calculations the tensor effects are irrelevant when all the spin-orbit particle levels are occupied.

The situation changes for ^{22}O and ^{24}O. In thes cases, the effect of the tensor force consists in lowering the position of the peaks of the response. It is possible to identify two different sources of this effect. A first one is present already at the HF level, as we can see by comparing nn and tn results. The second source is a genuine RPA effect, as we deduce by observing the tt results. Our tensor terms are attractive in the RPA description of the 1^+ excitation.

The effect observed in the tn results is due to a change of the s.p. neutron energies. In the case under investigation, the s.p. energies of interest are those of the $(1d_{5/2})^{-1}$ and the $(1d_{3/2})$ neutron levels. In our HF calculations, the inclusion of the tensor term enhances the value of the energy of the first state and lowers that of the second one, and this reduces the energy difference. Otsuka and collaborators [18, 19] pointed out an effect of the tensor force which produces a lowering of the energy differences between spin-orbit partner levels.

This effect appears in nuclei where not all the spin-orbit partner levels of a certain type of nucleons (protons or neutrons) are occupied and affects the s.p. energies of the nucleons of the other type. Therefore, in the two nuclei under investigation, the proton s.p. levels should be affected, as we have verified it happens in our HF calculations. In Ref. [7] we have investigated the presence, and the consequences, of this effect, which we called Otsuka effect, in various nuclei, including ^{22}O and ^{24}O. However, in the case we are discussing now, the changes of the proton s.p. energies have small effects on the main peak of the 1^+ excitation in ^{22}O and ^{24}O which is dominated by the neutron excitation indicated above. This means that in our results we do not observe the effect pointed out by Otsuka et al., but a similar one. In the present case, the s.p. energies which are modified are those of the nucleons of the same type of those where not all the spin-orbit partner levels are occupied.

The study of the tensor effect has been done also by investigating the electron scattering responses. We show in Fig. 5 the transverse 1^+ responses of ^{22}O calculated at the peak energy with and without tensor force, in both discrete and continuum RPA frameworks. We observe that in both type of calculations the tensor increases the responses at large q values. The analysis of the results of Fig. 3 indicates that the peak at $q = 2.7$ fm^{-1} is lowered by the presence of proton excitations. Therefore the results of Fig. 5 indicate that the tensor force quenches the proton contribution, enhancing the role of the main neutron excitation. We have done analogous calculations in ^{24}O and we have observed similar effects.

The study of the 1^+ excitation we have just presented for the oxygen isotopes has been carried on also for the four calcium isotopes under investigation. The main features pointed out in the discussion regarding the oxygen isotopes have been found also in this case. The $B(\mathcal{M}1)\uparrow$ values of the ^{40}Ca and ^{60}Ca isotopes are orders of magnitude smaller than those obtained in ^{48}Ca and ^{52}Ca. In this case, the cause of the effect is the occupancy of the $1f$ spin-orbit partner s.p. levels. They are both empty in ^{40}Ca, and occupied in ^{60}Ca, while for the other two nuclei the $(1f_{7/2})^{-1}$ level is occupied, while the $(1f_{5/2})$ level is empty. The 1^+ transition between these two levels is allowed and this produces the increase of the strength of various order of magnitude in ^{48}Ca and ^{52}Ca. There is a small difference with respect to the oxygen case. In ^{24}O the $2s_{1/2}$ was occupied, but this did not produce other $0\hbar\omega$ 1^+ excitations. In ^{52}Ca the $(2p_{3/2})^{-1}$ is occupied, while its spin-orbit partner, the $(2p_{1/2})$ level is empty. In this nucleus, the transition between these two states adds another $0\hbar\omega$ component to the 1^+ excitation.

In analogy with the oxygen results, we have found that the total strengths of the DIPM and DTDA calculations are conserved, while the values of the total DRPA strengths are smaller than the two previous ones. In this last case, the inclusion of the tensor force further reduces the values of the total strengths, without exceptions. The same happens for CIPM and CRPA calculations. The calculations in calcium isotopes confirm that DRPA and CRPA produce peaks at the same excitation energies. Also the general effect of the residual interaction in RPA calculations has been confirmed. And finally, we have observed that also for the calcium isotopes the residual interaction moves the positions of the peaks at higher energies with respect to those obtained in IPM calculations.

We show in Fig. 6 the energy distributions of the $B(\mathcal{M}1)\uparrow$ strengths calculated with the D1S and D1ST interactions for the ^{48}Ca and ^{52}Ca nuclei. The comparison between these results illustrates the role of the tensor force. We do not show the results for ^{40}Ca and ^{60}Ca since, in this case, the effects of the tensor force are negligible, as it happens in ^{16}O and ^{28}O nuclei. We recall that in these nuclei, all the spin-orbit partner levels are fully occupied. In Fig. 6 we used a logarithmic scale to emphasize the widths of the peaks. The role of the tensor force is analogous to that pointed out in the discussion of Fig. 4. The position of the peak is lowered when the tensor force is considered. In the case of the ^{48}Ca nucleus, the size of the effect is large enough to push the main resonance peak below the particle emission threshold. We should remark that when the D1M interaction is used, the peak energy is below the particle emission threshold already in the calculation without tensor force. Its inclusion pushes further down the position of the peak.

The role of the tensor force is more clear in ^{52}Ca where the main excitation peak is always above threshold as it is shown in the panel (b) of Fig. 6. In this case, it is possible to observe in a very clean way the lowering of the peak positions induced by the tensor force. The peaks below the particle emission threshold shown by the discrete calculations are produced by the $[(2p_{1/2})(2p_{3/2})^{-1}]$ neutron transition. The main peaks, in the continuum, are instead dominated by the $[(1f_{5/2})(1f_{7/2})^{-1}]$ neutron transition. We have verified that also in this case, as discussed in detail for the oxygen isotopes, the global effect of the tensor force is produced by the sum of an effect on the s.p. energies and a genuine effect in the RPA calculation.

Experimentally, the 1^+ excitation in ^{48}Ca has been studied by using inelastic electron scattering [20–22]. This investigation has identified an isolated 1^+ excitation at 10.23 MeV,

with $B(\mathcal{M}1)\uparrow = 4.0 \pm 0.4\ \mu_N^2$. Our RPA calculations generate the main 1^+ peak at 10.15 MeV, when the D1S force is used, and at 8.56 MeV, when we consider the D1ST force. The corresponding $B(\mathcal{M}1)\uparrow$ values related to the main peaks are, respectively, 9.72 and 9.27, in μ_N^2 units. The values of the total, integrated, $B(\mathcal{M}1)\uparrow$ strengths are 10.66 and 10.07 μ_N^2 MeV, respectively, to be compared with the almost 12 μ_N^2 MeV predicted by the IPM model. The CRPA calculations done with the D1M and D1MT interactions generate peaks at 9.25 and 8.58 MeV with $B(\mathcal{M}1)\uparrow$ values of 10.31 and 9.99 μ_N^2 , respectively.

The inclusive (e, e') transverse responses, obtained by using the RPA wave functions in the peak energy, are compared in Fig.7 with the experimental data of Ref. [21]. In this figure, we show continuum and discrete results obtained without tensor, and also the DRPA result obtained by using the tensor force. The CRPA result with the tensor force is absent, since, in this case, the main peak is below the particle emission threshold.

We remark the agreement of the three calculations in the two peaks at lower momentum values. In analogy to what we have observed in the case of the ^{22}O nucleus, the differences between the various results arise at momentum transfer values larger than 2 fm^{-1}. These differences are related to the proton excitations, as we have verified by applying in this case the same type of investigation done with the results of Fig. 3. We found, again, that the contribution of these excitations is smaller in CRPA than in DRPA wave functions. Also in the present case, the contibution of the proton excitations is further reduced by the tensor force.

The comparison with the experimental data of Ref. [21] indicate that our results overestimate the data of the first peak. At $q = 0.4$ fm^{-1}, we need quenching factors of 0.48 and 0.51, respectively, for the D1S and D1ST results. These values are similar to those of the quenching factors necessary to reproduce the experimental $B(\mathcal{M}1)\uparrow$ value. The application of a global quenching factor to our responses would spoil the agreement with the data in the second peak. Evidently, the physics behind the disagreement between experimental and calculated responses is momentum transfer dependent, and cannot be described by a single number, i. e. by using a quenching factor.

B. Magnetic excitations beyond the dipole

In this section, we present our results for the magnetic excitations with angular momentum larger than 1. We shall concentrate on the 2^- and 3^+ excitation modes. These two modes are composed by p-h excitations with intrinsic different characteristics. The 2^- mode is composed by p-h transitions between different major shells. On the contrary, in the 3^+ mode p-h excitations within the same major shell are allowed. We investigate whether this difference produces remarkable effects on observables.

The study on the total strengths presented in Table I for the 1^+ excitation in oxygen isotopes has been repeated also for the 2^- and 3^+ excitations in both oxygen and calcium isotopes. We found results similar to those presented in Table I. Within the limits of the numerical accuracy the values of the DIPM and DTDA total strengths coincide. In RPA calculations (both discrete and continuous) the total $B(\mathcal{M}2)\uparrow$ and $B(\mathcal{M}3)\uparrow$ values are smaller than those obtained in DIPM calculations. The inclusion of the tensor force produces a further lowering of these values.

We make now a more detailed analysis of the strength distributions of these excitation modes. We compare in Fig. 8 the results obtained in discrete and continuum RPA calculations for the 2^- excitation in the oxygen isotopes, when the D1S interaction is used. For all the isotopes considered we observe a good agreement between the position of the peaks in discrete and continuum results. The size of the $B(\mathcal{M}2)\uparrow$ strength for the ^{16}O and ^{28}O is comparable with that of the other two isotopes, contrary to what we found for the 1^+ excitation.

The effect of the tensor force is shown in Fig. 9 where the CRPA results obtained with the D1S interaction, the same shown in Fig. 8, are now compared with those obtained by using the D1ST force, indicated here by the dashed lines. We observe that the strengths are concentrated in three different regions. A first one between 10 and 16 MeV, a second one between 16 and 20 MeV, and a third one around 25 MeV. The ^{22}O, ^{24}O and ^{28}O nuclei show some strength also below 10 MeV that is not present in the ^{16}O case.

The excitations between 10 and 15 MeV are dominated by the $[(1d_{5/2})(1p_{1/2})^{-1}]$ proton transitions. The calculations with and without tensor predict almost identical excitation energies for these resonances in the ^{16}O and ^{28}O nuclei, while for the ^{22}O and ^{24}O nuclei the resonances of the calculations with D1ST have larger energies than those obtained with

D1S. This is a consequence of the Otsuka effect of the tensor force on the s.p. energies. In the ^{22}O and ^{24}O, because of the occupancy of the neutron $(1d_{5/2})^{-1}$ s.p. level, the energy of the proton $(1p_{1/2})^{-1}$ level is lowered while that of the $(1d_{5/2})$ one is enhanced. The transition between these two states requires more energy and this implies an increase of the excitation energy of the nucleus. Because all the s.p. spin-orbit partner levels are occupied in ^{16}O and ^{28}O nuclei, the effect we have just described is always compensated by another one similar but of different sign. For this reason, in these latter nuclei, the energies obtained in calculations with and without tensor almost coincide. The resonances observed at higher energies are composed by various p-h excitations and it is difficult to identify a dominant transition. The strength below 10 MeV in the three heavier oxygen isotopes is produced by excited states dominated by the $[(2p_{3/2})(1d_{5/2})^{-1}]$ neutron transition.

Experimentally, the 2^- excitation of ^{16}O has been studied with electron scattering [23]. In this investigation a total $B(\mathcal{M}2)\uparrow$ strength of 1052 ± 272 μ_N^2 fm^2 has been found. Our calculations predict larger values, around 1860 μ_N^2 fm^2. In Refs. [24, 25] results of RPA calculations predicting total strengths of 1204 μ_N^2 fm^2 are quoted. We have also calculated the 2^- excitation by using a phenomenological model with the Landau-Migdal residual interaction proposed in Ref. [26], and we have obtained a total strength of 1670 μ_N^2 fm^2.

The investigation done for the 2^- excitation has been repeated for the 3^+ mode. We summarize in Fig. 10 our results regarding the energy distribution of the $B(\mathcal{M}3)\uparrow$ strength for the oxygen isotopes. In the panels (a), (b), (c) and (d) we compare discrete (dashed vertical lines) and continuum (full lines) RPA calculations done with the D1S interaction. In the other two panels we compare the CRPA results obtained with the D1S (full lines) and the D1ST (dashed curves) interactions for the ^{22}O and ^{24}O isotopes. For the other two oxygen isotopes under investigation the results obtained with and without tensor almost overlap, as observed for the 1^+ and 2^- cases.

The results of Fig. 10 indicate a good agreement between the position of the peaks obtained in discrete and continuum calculations. With the exception of the ^{28}O nucleus, the main part of the strength is located above 20 MeV. The main peaks are dominated by the $[(1f_{7/2})(1p_{1/2})^{-1}]$ proton transition. The difference between the positions of the peaks obtained with and without tensor is due mainly to the Otsuka effect. In these two nuclei the occupation of the neutron $(1d_{5/2})^{-1}$ level decreases the energy value of the proton $(1p_{1/2})^{-1}$ level, and enhances that of the $(1f_{7/2})$ one. The increase of the bare p-h energy difference

induces a difference in the position of the peaks obtained in the CRPA calculations.

The study on the 2^- and 3^+ has been carried on also for the calcium isotopes and we show in Fig. 11 the energy distribution of the $B(\mathcal{M}2)\uparrow$ excitation in these nuclei. The structure of the figure is analogous to that of Fig. 10. In the four upper panels we compare discrete and continuum RPA results obtained with the D1S interaction and in the two lower panels we show the effect of the tensor force for the two isotopes where this effect is remarkable.

As always observed in the previous cases, we remark a good agreement between the position of the peaks obtained in discrete and continuum results. In all the responses we identify a sharp excitation at energies below 10 MeV and wider, and more fragmented, excitations around 15 MeV.

The excitation below 10 MeV is dominated by a specific p-h excitation, the $[(1f_{7/2})(1d_{3/2})^{-1}]$ proton transition. The energy of this excitation is below the particle emission threshold for the ^{40}Ca and ^{48}Ca nuclei. The comparison of the results obtained with and without tensor can be explained by means of the Otsuka effect absent in the ^{40}Ca and ^{60}Ca isotopes. In ^{48}Ca and ^{52}Ca, where the neutron $(1f_{7/2})^{-1}$ state is occupied while its spin-orbit partner level is empty, the tensor force, acting between this state and the proton states, lowers the energy of the proton $(1d_{3/2})^{-1}$ level, and enhances that of the $(1f_{7/2})$ one, increasing the energy difference between these two levels, with the obvious consequences on the nuclear excitation energies evident in the panels (e) and (f) of the figure.

The resonances at about 15 MeV have more collective character. In all the isotopes we have considered, these resonances are dominated by the same proton and neutron s.p. excitations, which are not related to the neutron excess of some of the isotopes considered. This indicates a collective common feature of all the nuclei under consideration.

An experimental study of the 2^- excitation in the ^{48}Ca nucleus has been carried on with electron scattering [25]. In this work, the study of the $B(\mathcal{M}2)\uparrow$ energy distribution has been limited to excitation energies smaller than 15 MeV (see Fig. 11 of Ref. [25]). The experimental strength shows a sharp peak at about 8 MeV, and broader structures at 12 and 15 MeV. The experimental value of the energy weighted sum rule deduced from Fig. 3 of Ref. [25] is about $(17 \pm 2) \cdot 10^3$ μ_N^2 MeV fm^2. By integrating up 16 MeV our $B(\mathcal{M}2)\uparrow$ continuum strengths we obtain, for the energy weigthed sum rule, the values of 29.89 and 24.87 in 10^3 μ_N^2 MeV fm^2 units, for the D1S and D1ST interactions, respectively. Extending the integral up to 30 MeV we obtain, respectively, 59.71 and 53.54 in 10^3 μ_N^2 MeV fm^2 units.

These values are in agreement with the RPA results of $52.4 \cdot 10^3$ μ_N^2 MeV fm^2, presented in Ref. [25]. In this reference it is shown that an improvement of the description of the experimental data is obtained when 2p-2h excitations are considered in RPA calculations. In any case, we should remark that the position of the peaks is not changed by the 2p-2h calculations.

The results of our calculations for the 3^+ excitations in calcium isotopes are shown in Fig. 12 whose structure is analogous to that of the previous two figures. Also in this case, we remark the agreement between the position of the peaks obtained in the discrete and continuum RPA calculations. The size of the $B(\mathcal{M}3) \uparrow$ strengths is analogous in all the isotopes considered. The strengths are mainly concentrated above 20 MeV, indicating that they are mainly generated by $2\hbar\omega$ excitations, i.e. transition between levels belonging to two major shells. In the three heavier isotopes, some strength below 10 MeV is present. This is produced by the $0\hbar\omega$ excitations of neutrons occupying the f s.p. levels.

Also in this case, the tensor force has no effects on the responses of the two nuclei where all the spin-orbit partner levels are occupied, i. e. ^{40}Ca and ^{60}Ca. For this reason, in the two lower panels, we show only the results related to ^{48}Ca and ^{52}Ca, where we found a remarkable effect. A detailed study of the resonances indicates that the shift between the peak positions is mainly due to the Otsuka effect.

V. CONCLUSIONS

In this article we have presented results of discrete and continuum self-consistent RPA calculations of magnetic excitations of some spherical oxygen and calcium isotopes. The calculations have been done by using the finite-range D1S and D1M interactions of Gogny type whose parameter values have been chosen by fitting global properties, mainly binding energies and radii, of more than thousand nuclei [4–6]. We also used two new interactions, D1ST and D1MT, obtained by adding a tensor-isospin term to the D1S and D1M forces [7].

As expected, the more striking result emerging from our calculations is related to the 1^+ excitation. The strengths of this excitation in nuclei where all the spin-orbit partner levels are occupied are orders of magnitude smaller than those in nuclei where one of the spin-orbit partner levels is empty. In this latter group of nuclei, a spin-flip transition between the two spin-orbit partner levels is allowed. This difference between the responses of the two groups

of nuclei is typical of the 1^+ excitation. The sizes of the 2^- and 3^+ responses have similar magnitudes in all the nuclei investigated, even in the 3^+ states where the same spin-flip transitions dominating the 1^+ excitation are present.

Our study indicates that, in general, magnetic excitations are more related to the s.p. structure of the nucleus than to collective effects. We found some indications of collectivity in the 2^- and 3^+ responses around 20-25 MeV in the oxygen isotopes, and at slightly smaller energies in the calcium isotopes. In any case, the main magnetic excitations are dominated by s.p. transitions. This does not mean that the effect of the residual interaction is negligible. The residual interaction moves the peak positions with respect to those of the IPM, and adds to the main p-h component also the contributions of other p-h transitions. This weaker components change the RPA wave function, and produce effects which show up at high momentum transfer values, above 2 fm^{-1}.

Since in magnetic excitations the residual interaction produces effects which can be treated as perturbations with respect to the main IPM response, it is possible to isolate the role of the various terms of the interaction. This feature has allowed a detailed investigation of the tensor-isospin term of the residual interaction. We have observed that relevant tensor effects are present only in those nuclei where not all the spin-orbit partner levels are occupied. In these nuclei, the effects of the tensor term of the interaction are active in both HF and RPA calculations. The tensor force changes the values of the s.p. energies. The effect pointed out by Otsuka and collaborators [18, 19] affects nucleons of different type. In our calculations, we found a similar effect acting also between nucleons of the same type. We have identified the consequences of the genuine Otsuka effect, and of its analogous, in ^{22}O, ^{24}O, ^{48}Ca, ^{52}Ca nuclei. In addition to these effects on the s.p. energies and wave functions, the tensor force affects also the RPA calculations, mainly in those nuclei where not all the spin-orbit partner levels are occupied.

In our calculations, the effects of the tensor force act against those of the other terms of the interaction. We have discussed in detail the case of the 1^+ excitation, where the residual interaction moves the position of the main peaks at higher energies with respect to the IPM results. The modification of the s.p. energies due to the tensor lowers the value of the excitation energy, and the presence of the tensor in the RPA calculation further diminishes this value which at the end results to be close to the original IPM value. Furthermore, the study of the RPA wave functions in the peak position, used to calculate the electron scattering

transverse responses, indicates that the presence of the tensor decreases the contribution of the p-h components different from the dominant one.

The comparison with the few experimental data available indicates that our calculations describe reasonably well the position of the excited states but they overestimate the strength of the magnetic excitations. For example, the values of the $B(\mathcal{M}1)\uparrow$ strengths in ^{48}Ca are more than two times larger than those indicated by the experiment. This result is common to all the mean-field shell model and RPA calculations, and it is known in the literature as the quenching problem [24]. Also the comparison with the 2^- excitation data in ^{48}Ca [25] indicates the need of quenching. We should remark, however, that, in this case, we found a non negligible amount of strength beyond the maximum excitation energy explored by the experiment. We have pointed out, by comparing our 1^+ electron scattering responses in ^{48}Ca with the experimental one [21], the need of a momentum dependent quenching factor to reproduce the data. This indicates that the physics behind the quenching effects is rather involved, and cannot be simulated by a simple reduction factor.

Another indication of the need of extending the traditional RPA approach is coming from the experimental observation of non negligible $B(\mathcal{M}1)\uparrow$ strength in ^{16}O and ^{40}Ca [23, 27]. We have already mentioned that, in our approach, the $B(\mathcal{M}1)\uparrow$ strength is negligible for nuclei with all spin-orbit partner levels occupied. Experimentally, a $B(\mathcal{M}1)\uparrow$ strength of about 1.0 μ_N^2 has been identified in ^{16}O [23] and of about 1.2 μ_N^2 in ^{40}Ca [27]. The description of these non-negligible strengths have been explained by considering 2p-2h excitations [28, 29].

The study of magnetic excitations in medium-heavy nuclei having a relatively simple structure offers the opportunity to obtain information about some basic nuclear effects, such as shell closure, tensor force, spin and orbital terms of the electromagnetic operator, and correlations. The new radioactive ion beams accelerators allow the production of unstable nuclei such as those we have investigated in our paper. The further implementation of electron scattering facility [30–32] would be extremely useful for this type of investigations.

Acknowledgments

This work has been partially supported by the PRIN (Italy) *Struttura e dinamica dei nuclei fuori dalla valle di stabilità*, by the Spanish Ministerio de Ciencia e Innovación (Contract Nos. FPA2009-14091-C02-02 and ACI2009-1007) and by the Junta de Andalucía (Grant No.

FQM0220).

[1] V. De Donno, G. Co', M. Anguiano, A. M. Lallena, Phys. Rev. C 83 (2011) 044324.

[2] V. De Donno, M. Anguiano, G. Co', A. M. Lallena, Phys. Rev. C 84 (2011) 03706.

[3] F. Chappert, Nouvelles paramétrisation de l'interaction nucléaire effective de Gogny, Ph.D. thesis, Université de Paris-Sud XI (France), http://tel.archives-ouvertes.fr/tel-001777379/en/ (2007).

[4] F. Chappert, M. Girod, S. Hilaire, Phys. Lett. B 668 (2008) 420.

[5] J. F. Berger, M. Girod, D. Gogny, Comp. Phys. Commun. 63 (1991) 365.

[6] S. Goriely, S. Hilaire, M. Girod, S. Péru, Phys. Rev. Lett. 102 (2009) 242501.

[7] M. Anguiano, G. Co', V. De Donno, A. M. Lallena, Phys. Rev. C 83 (2011) 064306.

[8] J. Dechargè, D. Gogny, Phys. Rev. C 21 (1980) 1568.

[9] T. Sil, S. Shlomo, B. K. Agrawal, P. G. Reinhard, Phys. Rev. C 73 (2006) 034316.

[10] A. R. Edmonds, Angular momentum in quantum mechanics, Princeton University Press, Princeton, 1957.

[11] P. Ring, P. Schuck, The nuclear many-body problem, Springer, Berlin, 1980.

[12] J. E. Amaro, G. Co', A. M. Lallena, Ann. Phys. (N.Y.) 221 (1993) 306.

[13] A. Akmal, V. R. Pandharipande, D. G. Ravenhall, Phys. Rev. C 58 (1998) 1804.

[14] S. Gandolfi, A. Y. Illarionov, S. Fantoni, J. C. Miller, F. Pederiva, K. E. Schmidt, Mont. Not. R. Astron. Soc. 404 (2010) L35.

[15] J.-P. Delaroche, M. Girod, J. Libert, H. Goutte, S. Hilaire, S. Péru, N. Pillet, G. F. Bertsch, Phys. Rev. C 81 (2010) 014303.

[16] G. Co', V. De Donno, P. Finelli, M. Grasso, M. Anguiano, A. M. Lallena, C. Giusti, A. Meucci, F. D. Pacati, Phys. Rev. C submitted.

[17] J. Heisenberg, H. Blok, Ann. Rev. Nucl. Par. Sci. 33 (1983) 569.

[18] T. Otsuka, T. Suzuki, R. Fujimoro, H. Grawe, Y. Akaishi, Phys. Rev. Lett. 95 (2005) 232502.

[19] T. Otsuka, T. Matsuo, D. Abe, Phys. Rev. Lett. 97 (2006) 162501.

[20] W. Steffen, H.-D. Gräf, W. Gross, D. Meuer, A. Richter, E. Spamer, O. Titze, W. Knüpfer, Phys. Lett. B 95 (1980) 23.

[21] W. Steffen, H.-D. Gräf, A. Richter, A. Härting, W. Weise, U. Deutchmann, G. Lahm, R. Neuhausen, Nucl. Phys. A 404 (1983) 413.

[22] W. Knüpfer, B. C. Metsch, A. Richter, Phys. Lett. B 129 (1983) 375.

[23] G. Küchler, A. Richter, E. Spamer, W. Steffen, W. Knüpfer, Nucl. Phys. A 406 (1983) 473.

[24] S. Raman, L. W. Fagg, R. S. Hicks, Electric and magnetic giant resonances in nuclei, J. Speth ed., World Scientific, Singapore, 1991.

[25] P. von Neumann-Cosel, F. Neumeyer, S. Nishizaki, V. Yu. Ponomarev, C. Rangacharyulu, B. Reitz, G. Schrieder, D. I. Sober, T. Weindzoch, J. Wambach, Phys. Rev. Lett. 82 (1999) 1105.

[26] G. Co', A. M. Lallena, Nucl. Phys. A 510 (1990) 139.

[27] W. Gross, D. Meuer, A. Richter, E. Spamer, O. Titze, W. Knüpfer, Phys. Lett. B 84 (1978) 296.

[28] A. Arima, D. Strottman, Phys. Lett. B 96 (1980) 23.

[29] S. Kamerdzhiev, J. Speth, G. Tertychny, Phys. Rep. 393 (2004) 1.

[30] T. Suda, et al., Phys. Rev. Lett. 102 (2009) 102501.

[31] T. Suda, Journal of Physics: Conference Series 267 (2011) 012088.

[32] A. N. Antonov, et al., Nucl. Inst. Met. A 637 (2011) 60.

		D1S	D1ST	D1M	D1MT
^{22}O	DIPM	8.796	8.866	8.803	8.814
	DTDA	8.796	8.866	8.803	8.814
	DRPA	7.618	7.155	7.887	7.581
	CIPM	8.106	7.890	8.106	7.927
	CRPA	6.225	5.599	6.385	5.906
^{24}O	DIPM	8.438	8.425	8.435	8.432
	DTDA	8.438	8.425	8.435	8.432
	DRPA	7.300	6.782	7.548	7.242
	CIPM	8.435	8.437	9.168	8.478
	CRPA	6.285	6.643	6.497	6.400

Table I: Total $B(\mathcal{M}1)\uparrow$ strengths in μ_N^2 MeV units, obtained in discrete and continuum calculations with various interactions for the ^{22}O and ^{24}O nuclei.

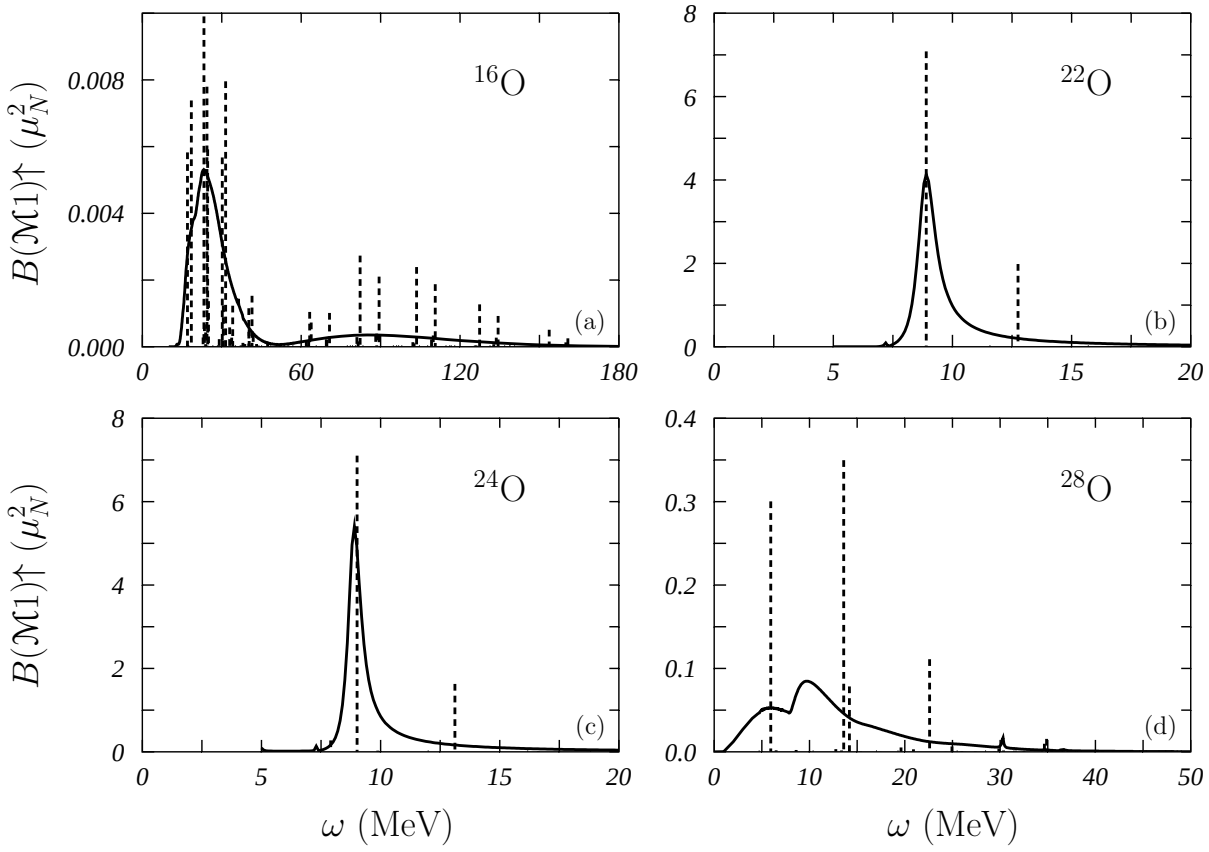

Figure 1: $B(\mathcal{M}1)\uparrow$ values obtained with the D1S interaction for the oxygen isotopes under investigation as a function of the excitation energy. The full lines show the CRPA results, while the vertical dashed lines indicate the DRPA results.

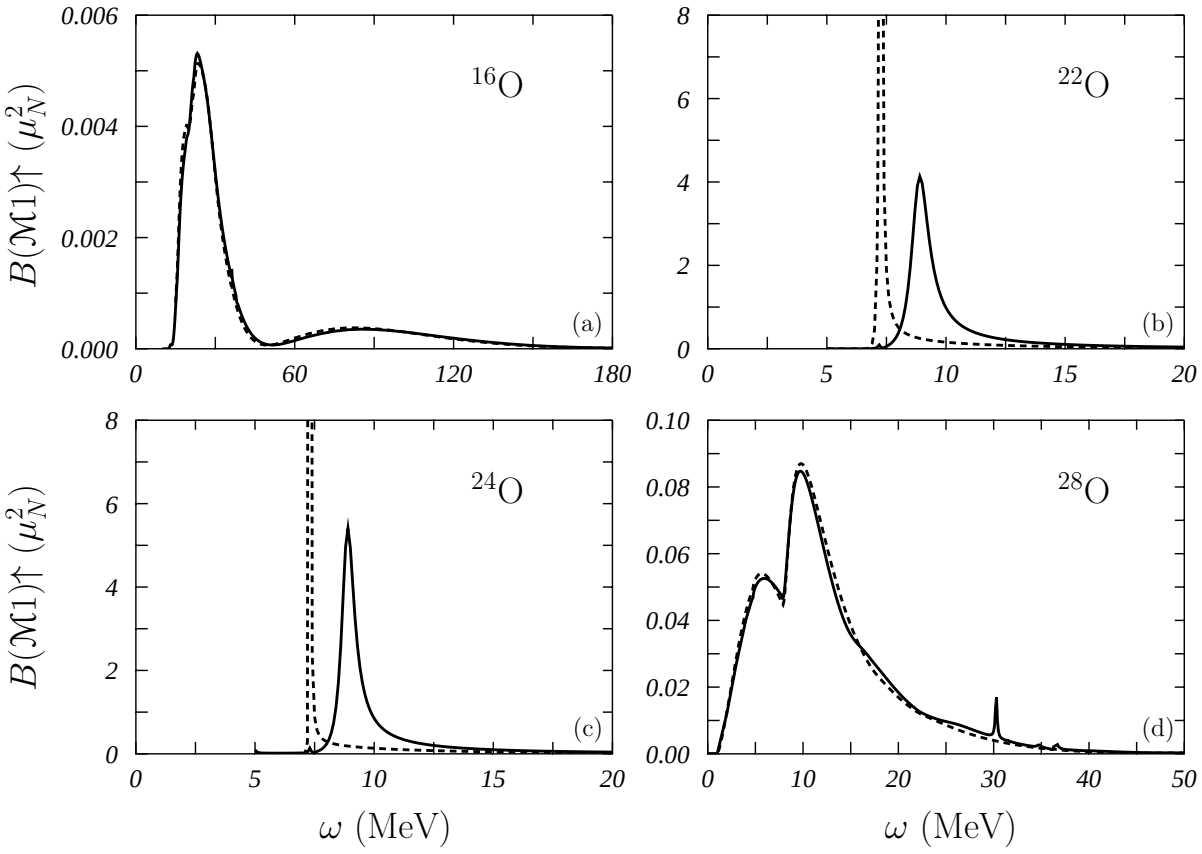

Figure 2: $B(\mathcal{M}1)\uparrow$ values obtained with the D1S interaction for the oxygen isotopes under investigation as a function of the excitation energy. The full lines show the CRPA results, while the dashed curves the CIPM results.

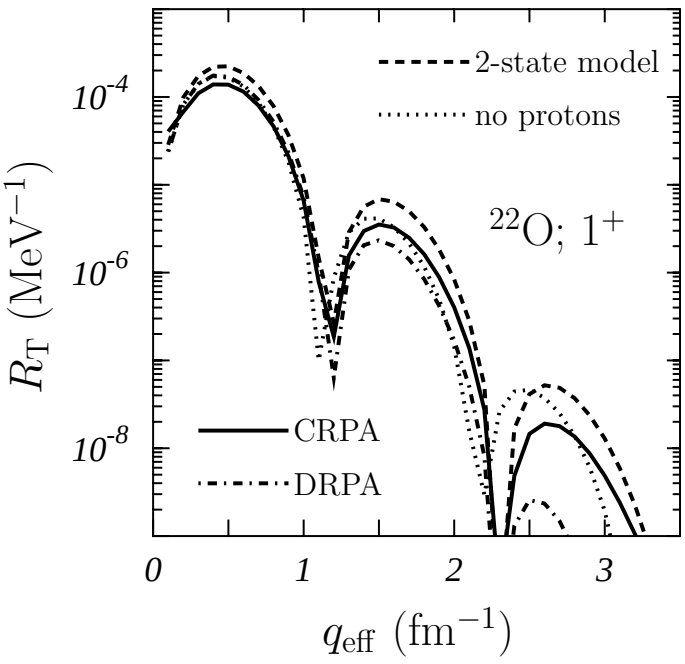

Figure 3: Transverse response of inelastic electron scattering 1^+ excitation in ^{22}O at the peak energy as a function of the effective momentum transfer. The DRPA and CRPA results obtained with the D1S force are compared. The dashed curve has been obtained by considering only the two main neutron p-h excitations in a DRPA calculation. The dotted curve corresponds to a DRPA calculation where all the proton excitations have been eliminated.

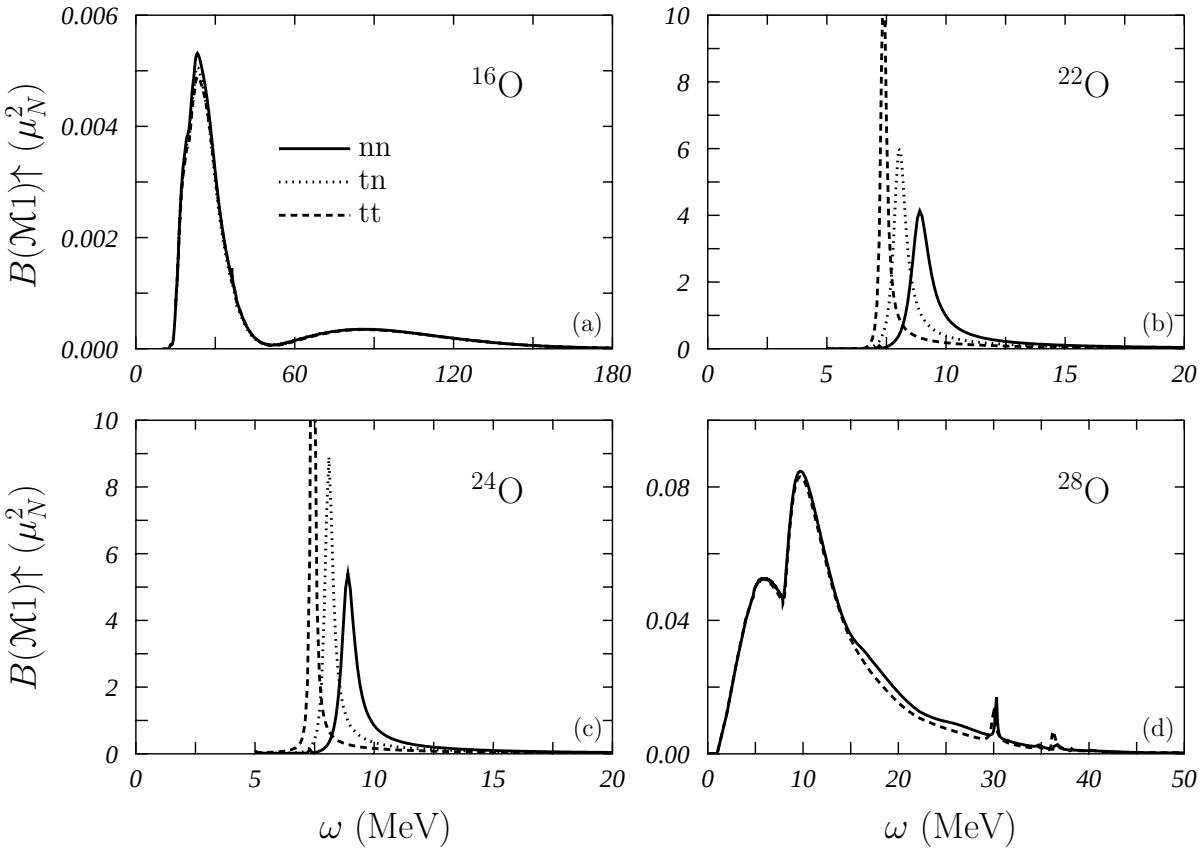

Figure 4: The CRPA results for the $B(\mathcal{M}1)\uparrow$ strengths of the oxygen isotopes under investigation as a function of the excitation energy. The full lines, already shown in Fig. 1 and 2, and here labelled nn, indicate the results obtained with the D1S interaction in both HF and RPA calculations. The dotted lines, labelled tn, have been obtained by using the D1ST interaction in the HF calculation and the D1S force in the CRPA ones. The dashed lines, labelled tt show the results obtained by using the D1ST interaction in both HF and RPA calculations.

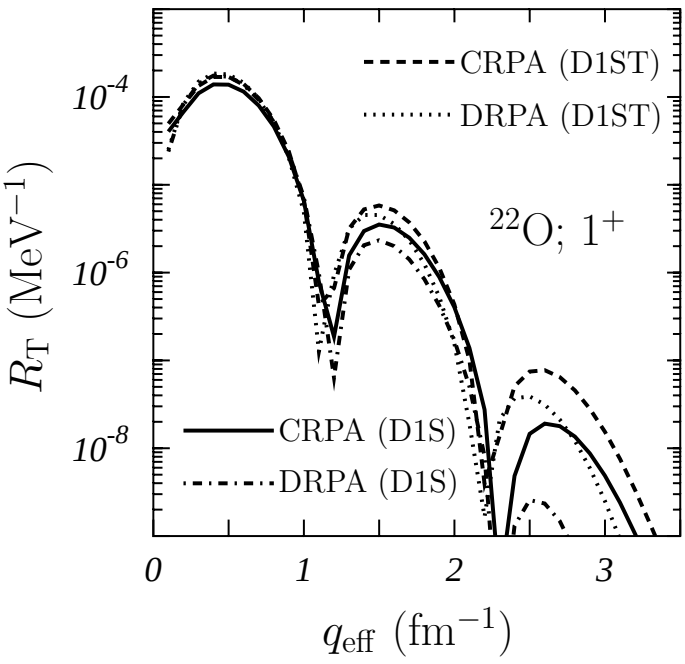

Figure 5: Transverse response of the inelastic electron scattering 1^+ excitation in the ^{22}O nucleus at the peak energy as a function of the effective momentum transfer. We compare discrete and continuum RPA results obtained with and without tensor force.

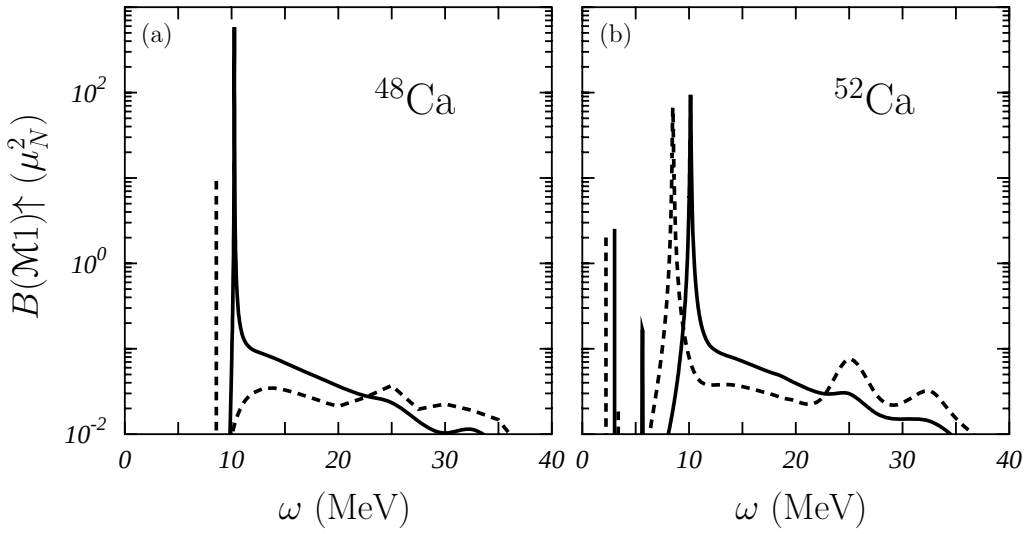

Figure 6: Energy distribution of the $B(\mathcal{M}1)\uparrow$ strength for two calcium isotopes. Full and dashed curves indicate the CRPA results obtained with D1S and D1ST interactions, respectively.

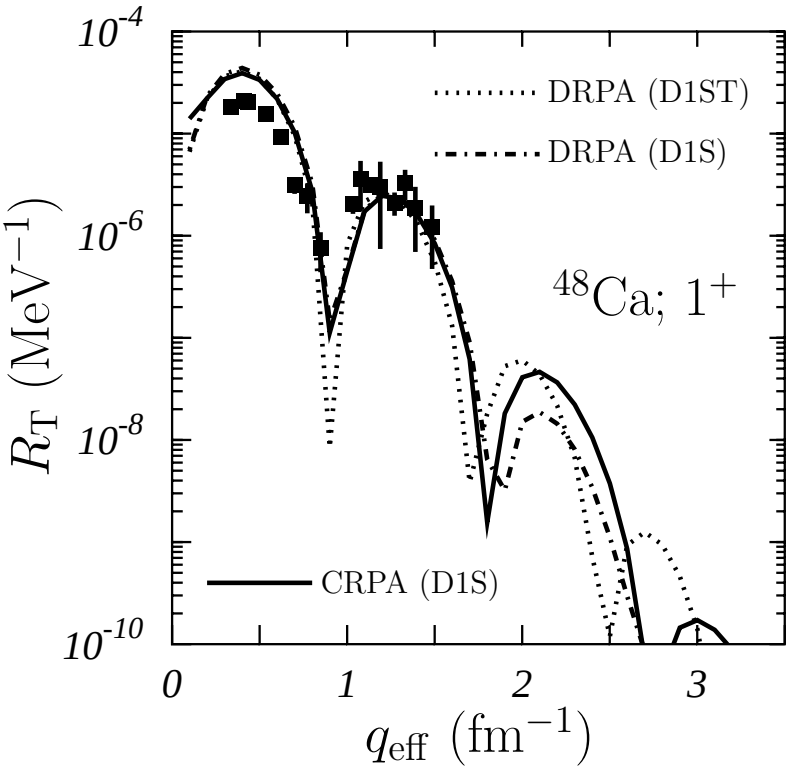

Figure 7: Transverse responses of the inelastic electron scattering for the 1^+ excitation in the ^{48}Ca nucleus at the peak energy as a function of the effective momentum transfer. We show the DRPA and CRPA results obtained with the D1S interaction and the DRPA result obtained with the D1ST interaction. The experimental data are from Ref. [21].

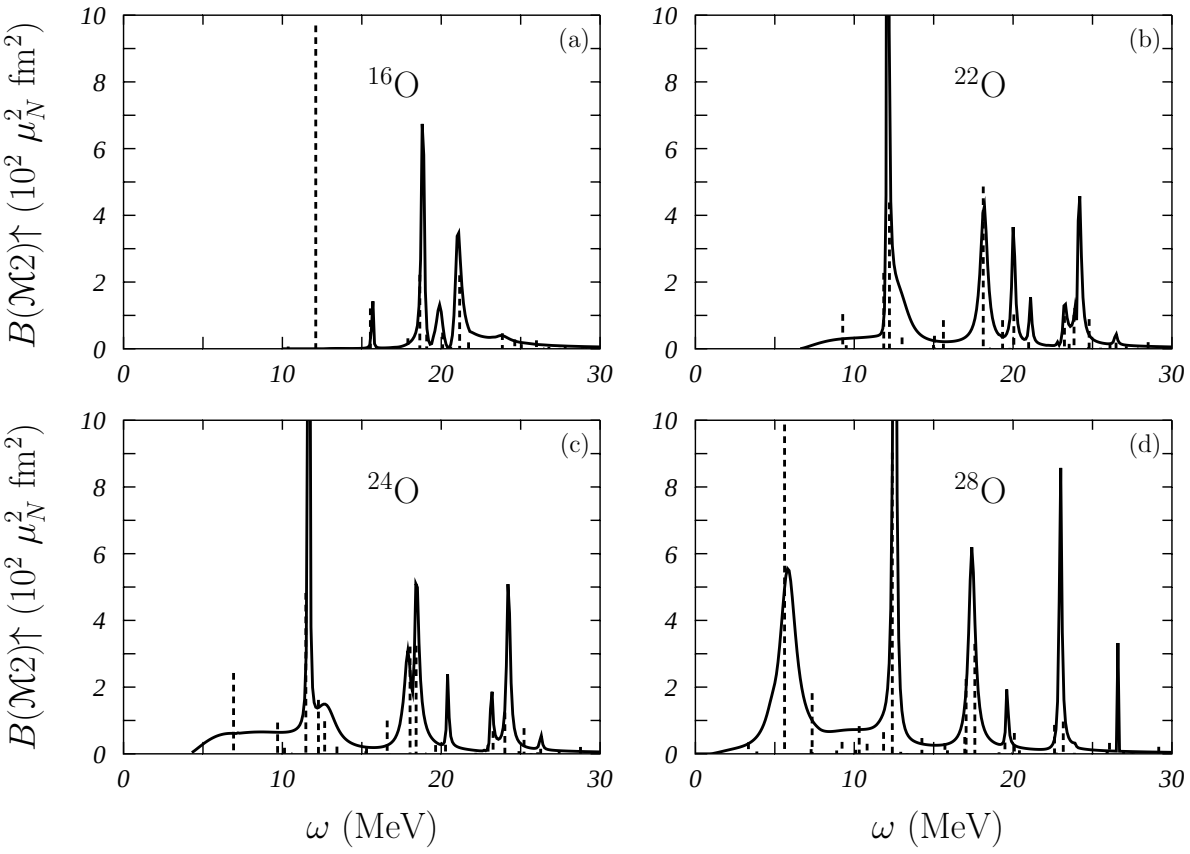

Figure 8: The same as Fig. 1 for the $B(\mathcal{M}2)\uparrow$ values.

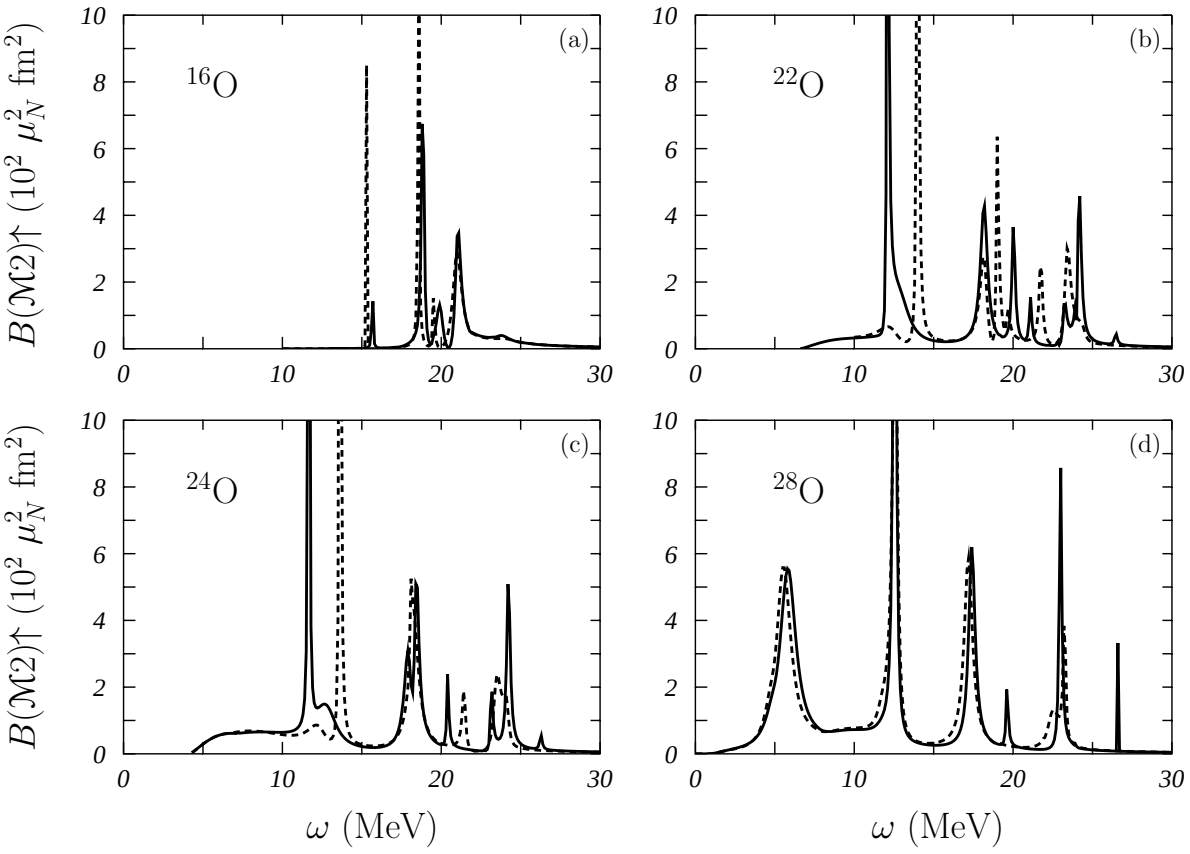

Figure 9: $B(\mathcal{M}2)\uparrow$ values for the four oxygen isotopes under investigation as a function of the excitation energy. The full and the dashed curves show the CRPA results obtained, respectively, with the D1S and D1ST interactions.

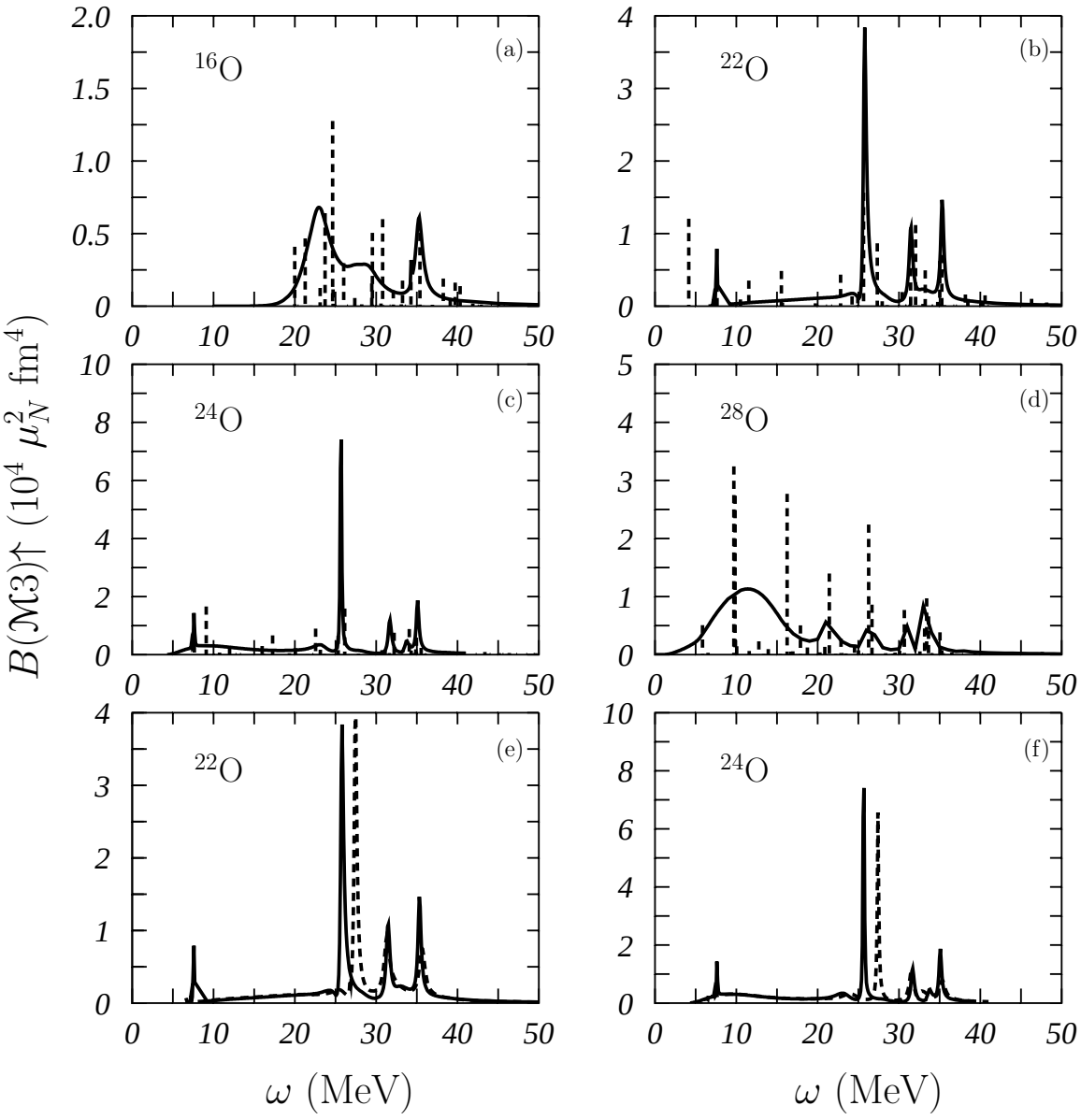

Figure 10: $B(\mathcal{M}3)\uparrow$ values for the oxygen isotopes under investigation as a function of the excitation energy. In panels (a)-(d) we compare DRPA, vertical lines, and CRPA, full lines, results obtained with the D1S interaction. For the ^{22}O and ^{24}O isotopes only, we compare, in the panels (e) and (f), the CRPA results obtained with the D1S and D1ST interactions indicated, respectively, by the full and dashed curves.

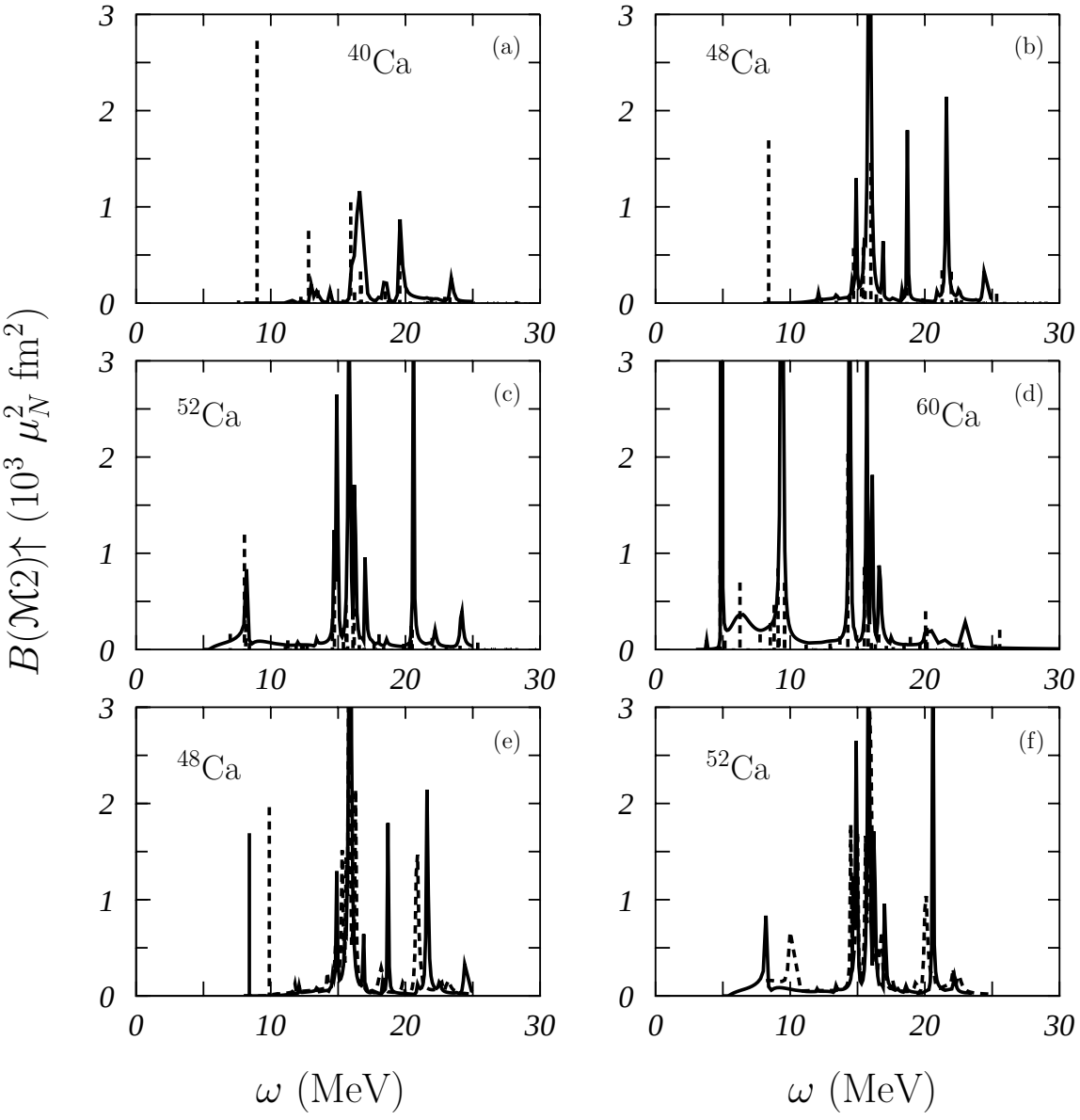

Figure 11: The same as Fig. 10. In this case we present the results of the $B(\mathcal{M}2)\uparrow$ values for the calcium isotopes under investigation.

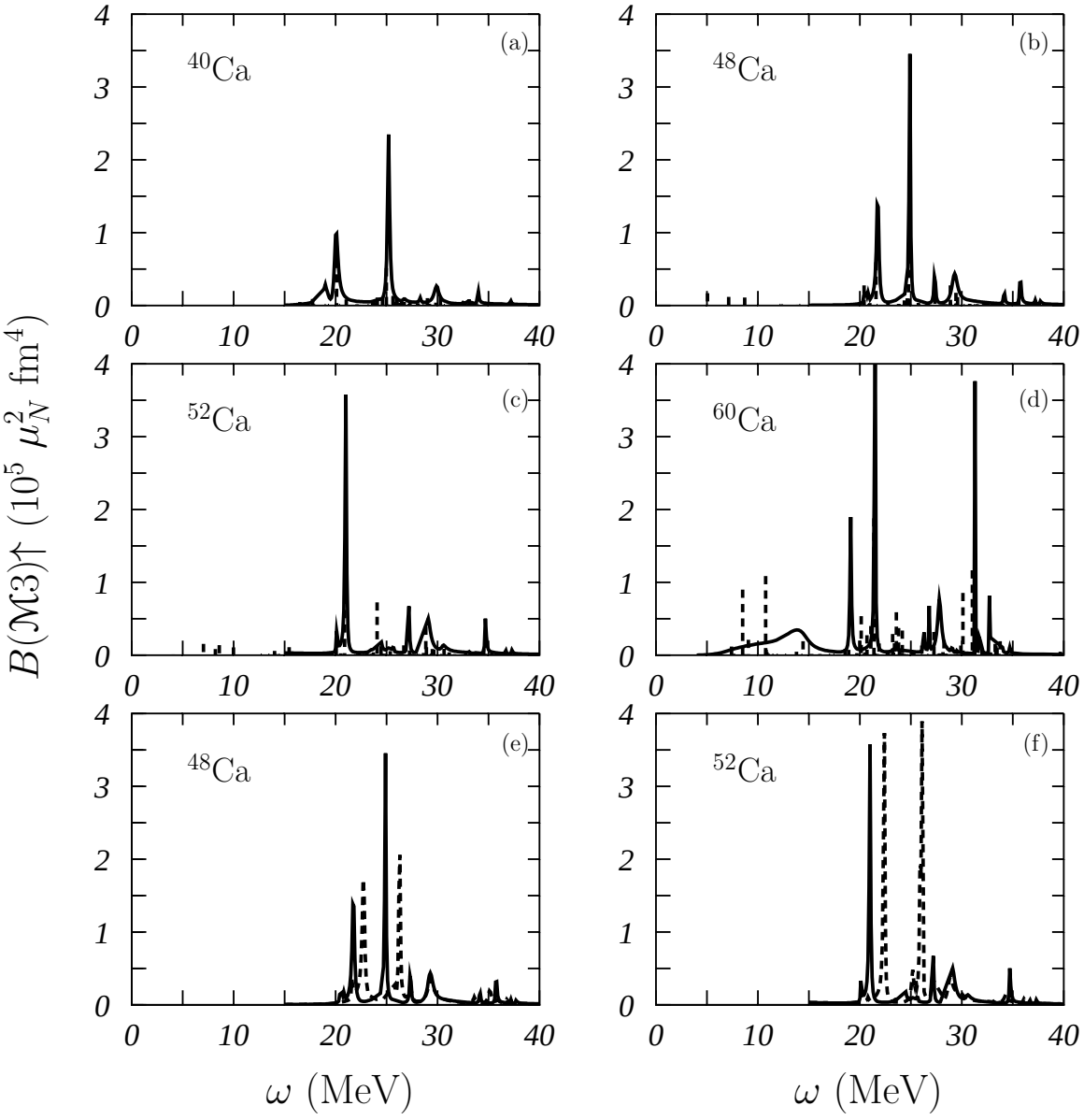

Figure 12: The same as Fig. 11 for the $B(\mathcal{M}3)\uparrow$ values.